JACS
JOURNAL OF THE AMERICAN CHEMICAL SOCIETY
pubs.acs.org/JACS
Article

Substrate-Induced One-Dimensional Borophene-Silver Hybridization

Qian Gao,[#] Wenbin Li,[#] Caiyun Chen, Kehui Wu, Zhenpeng Hu,[*] and Lan Chen[*]

Cite This: https://doi.org/10.1021/jacs.5c23239
Read Online
ACCESS | Metrics & More | Article Recommendations | Supporting Information

ABSTRACT: The performance of devices based on two-dimensional (2D) materials is fundamentally limited by their contacts with metal electrodes. Thus, the realization of covalent bonding between 2D materials and metal electrode presents a potential solution. Here, we fabricate a novel type of interface between 2D boron sheet (borophene) with one-dimensional (1D) silver chains on Ag(111) surface. Using scanning tunneling microscopy (STM) and density functional theory (DFT), the atomic structures of the boron-silver interface are identified, which indicate 4-fold superlattice modulation with a period of ∼1.20 nm along the borophene edges due to the compressive strain field at the interface. Electronic structure analysis reveals charge transfer and the formation of polar covalent Ag−B bonds at the interface, facilitating efficient electron injection reminiscent of an Ohmic contact. This work establishes a substrate-enabled, stress-driven pathway for creating atomically precise 2D materials/metal interfaces, providing a model platform for exploring low-dimensional quantum phases and the fundamental interface engineering.

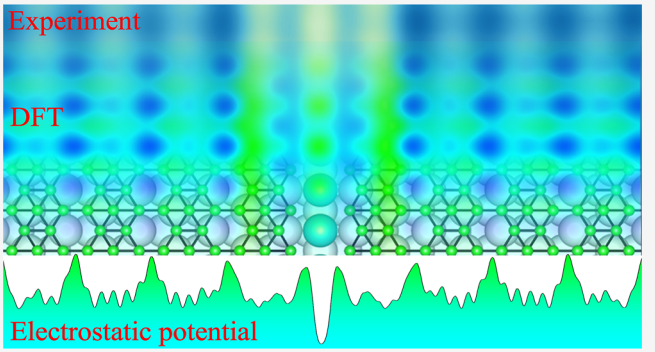

INTRODUCTION

The performance of any electronic device is ultimately governed by its interfaces, where carrier injection and transport are dictated by quantum-mechanical interactions.[1−3] For two-dimensional (2D) materials, forming low-resistance, atomically sharp contacts with metals remains a central challenge, as disordered interfaces and Fermi-level pinning often degrade device characteristics.[4,5] Borophene is a metallic 2D allotrope of boron with exceptional conductivity, anisotropic structure, and theoretically predicted exotic states,[6,7] which renders its contact with metals technologically significant and fundamentally distinct from conventional semiconductor-metal junctions. Unlike graphene, borophene can form strong directional bonds with metal atoms, suggesting the possibility of covalently coupled, low-dimensional (e.g., 1D/2D) interfaces that may overcome classic contact limitations.[8−12] However, the atomic-scale structure and bonding mechanism of such borophene-metal interfaces remain largely unexplored, in part due to the scarcity of well-defined experimental systems that realize coherent, epitaxial contact at the 1D/2D limit.

Borophene exhibits rich polymorphism and has been successfully synthesized on several metal substrates, including Ag(111),[13,14] Ag(110),[15] Ag(100),[16] Cu(100),[17] Cu(111),[18] Al(111),[19] Au(111),[20] and Ir(111).[21] The substrate plays a decisive role in stabilizing specific borophene phases through a synergistic balance of interfacial strain and electronic hybridization, which in turn dictates the resulting film morphology and crystalline quality. For instance, Cu(111) enables the growth of large-area, single-crystalline sheets via a step-edge-triggered mechanism,[18] whereas Al(111) stabilizes a distinct honeycomb phase.[19] Growth on Au(111) and Ir(111) proceeds through alternative pathways such as surface segregation and borazine decomposition, respectively.[20,21] In contrast, borophene grown on Ag(111) typically forms nanoislands or phase-mixed structures rather than extensive continuous films.[22−24] This specific growth mode, however, makes the Ag(111) substrate an exceptionally rich platform for atomic-scale interfacial studies. While prior research has extensively characterized borophene's intrinsic properties and long-range moiré superstructures, the atomic configuration and electronic role of the 1D line defects or domain boundaries (DBs) that naturally form between identically oriented domains have remained less explored. These intrinsic boundaries constitute embedded low-dimensional interfaces within the borophene sheet, and their detailed structure could provide critical insights into how substrate atoms participate in interfacial bonding, as well as how such atomic-scale participation modulates local electronic behavior.

Received: December 28, 2025
Revised: May 18, 2026
Accepted: May 26, 2026

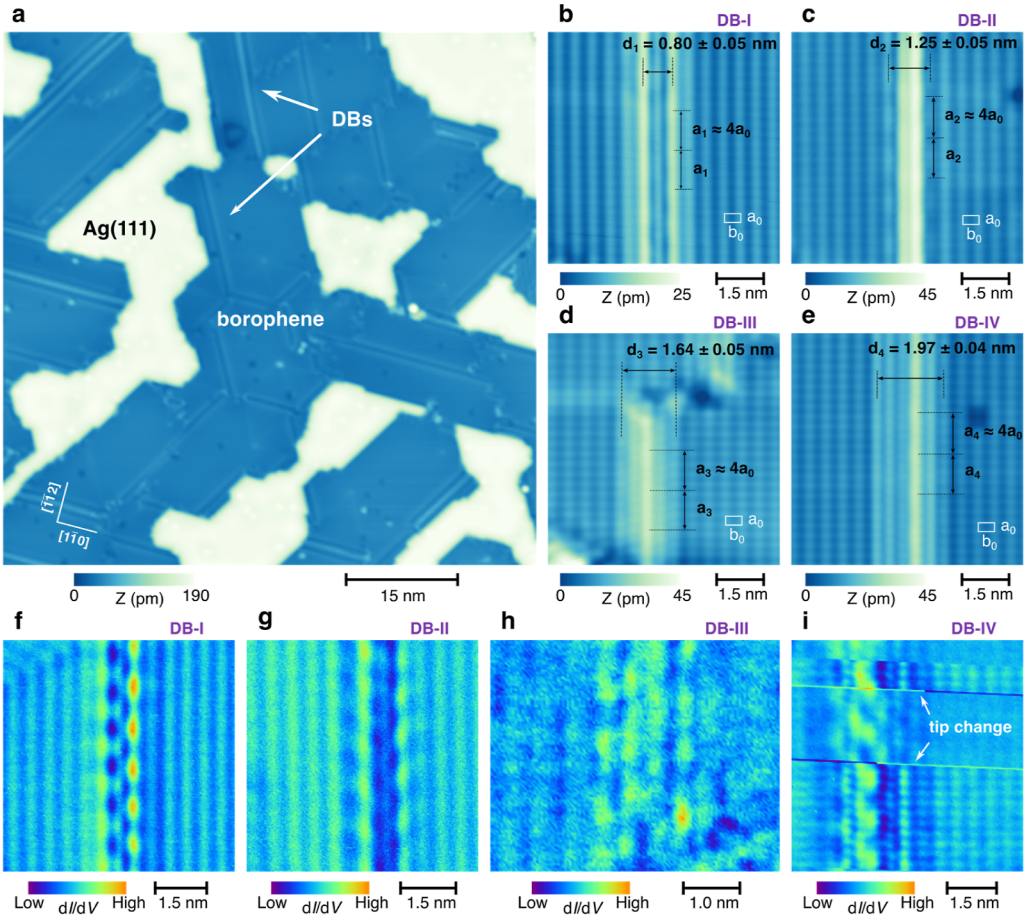

Figure 1. Four types of domain boundaries in borophene β_{12}-0° on Ag(111). (a) Large-scale STM topography of monolayer borophene β_{12}-0° showing multiple types of domain boundaries. (b–e) Atomically resolved STM images of the four distinct domain boundaries, labeled DB-I to DB-IV, respectively. (f–i) dI/dV maps of the four types domain boundaries acquired at selected sample biases reveal pronounced 4-fold superlattice modulations along the borophene β_{12}-0° chain direction. The scanning parameters are (a) V_{tip} = 1.0 V, I = 50 pA; (b) V_{tip} = 0.5 V, I = 100 pA; (c) V_{tip} = 0.2 V, I = 100 pA; (d) V_{tip} = 1.0 V, I = 200 pA; (e) V_{tip} = 1.0 V, I = 50 pA; (f) V_{tip} = 0.1 V, I = 50 pA; (g) V_{tip} = 0.2 V, I = 150 pA; (h) V_{tip} = 0.1 V, I = 50 pA; (i) V_{tip} = 0.2 V, I = 500 pA.

In this work, we investigated a series of line DBs in borophene β_{12} phase on Ag(111) surface using scanning tunneling microscopy (STM) and density functional theory (DFT) calculations, and identified a characteristic 4-fold superstructure modulation along the boundary direction. To elucidate this unusual modulation, we systematically performed DFT calculations on various possible DB structural models and found that the ordered line DBs and their associated superlattice modulations originate from the insertion of 1D Ag chains at the boundary. The four types of DBs can thus be interpreted as different arrangements between the inserted Ag chains and the neighboring boron chains. Our work of the atomic-scale investigation on borophene-metal interface provides new insights into how substrate atoms participate in the formation of 1D hybrid structures. This understanding deepens our knowledge of substrate-mediated epitaxial growth and provides a new perspective for designing atomically precise mixed-dimensional heterostructures with tailored interfacial properties, thereby establishing a model system for fundamental studies of low-dimensional interfaces.

RESULTS AND DISCUSSION

Configurations of Borophene β_{12}-0° Phase with Distinct Boundaries

The borophene β_{12} phase features a rectangular lattice with a lattice constant of $a_0 \approx 0.3$ nm, $b_0 \approx 0.5$ nm. According to previous experimental reports, it exhibits two distinct rotational orientations,[13,25] where the a-axis is either aligned along or rotated by 90° with the Ag [1$\bar{1}$0] direction, denoted by β_{12}-0° and β_{12}-90°. Figure 1a shows a typical STM morphology image of a pure β_{12}-0° submonolayer on Ag(111) substrate, which can be distinguished by the dark blue and bright regions, respectively. Notably, the borophene features distinctive straight boundaries along the a-axis direction (Ag [1$\bar{1}$0] direction). These differ from the previously studied twin boundaries that arise from the coalescence of misoriented domains.[24] The bright boundaries, in contrast, occur between domains of identical orientation and display a pronounced stronger contrast, suggesting a distinct underlying atomic structure. From the statistical result of extensive atomic-scale STM imaging, these DBs can be classified into four types, by their widths and atomic configurations, denoted by DB-I to DB-IV. High-magnification images (Figure 1b–e) reveal that all these boundaries exhibit chain-like structures, each with a

https://doi.org/10.1021/jacs.5c23239
J. Am. Chem. Soc. XXXX, XXX, XXX−XXX

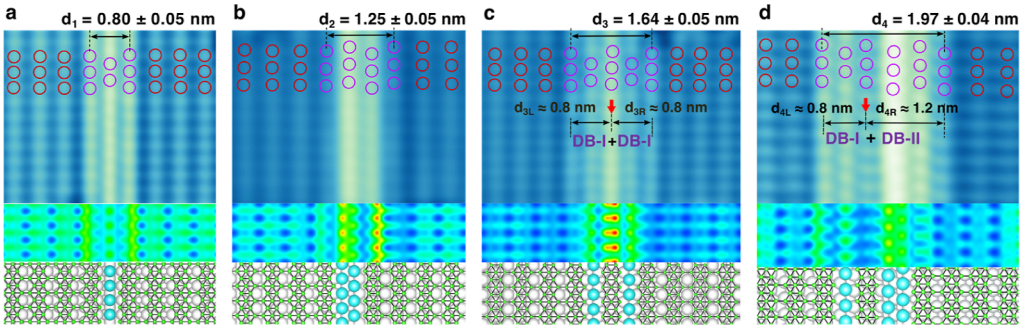

Figure 2. Comparison between experimental and simulated STM images for domain boundaries DB-I to DB-IV. (a–d) For each boundary type, the panels from bottom to top display the corresponding atomic structural model, the DFT-simulated STM image, and the experimental STM image. Atoms are color-coded as follows: green for boron, white for substrate Ag atoms, and cyan for Ag atoms within the boundary region. The excellent agreement between experiment and simulation validates the proposed atomic configurations of the boundaries. The scanning parameters for all experimental images are V_{tip} = 1.0 V, I = 200 pA. The simulated STM images were obtained at a sample bias of −1 V, consistent with the experimental imaging conditions.

characteristic morphology. As shown in Figures 1b–e and 2, in the STM images, the normal borophene β_{12}-0° appears as parallel atomic chains with a periodicity of a_0 and an interchain spacing of b_0, without any along-chain shift. In contrast, the DBs also exhibit the chain-like configuration with the same periodicity of a_0, but the adjacent chains are displaced by a half-a_0 shift and show a slightly smaller interchain distance. The edge chains, which form at the interface between the normal β_{12} and the half-a_0 shifted regions, demarcate each DBs. The width of each DB is then defined as the separation between these two edge chains, denoted as d_1 to d_4, respectively. Experimental measurements give d_1 = 0.80 ± 0.05 nm, d_2 = 1.25 ± 0.05 nm, d_3 = 1.64 ± 0.05 nm, and d_4 = 1.97 ± 0.04 nm. Including the edge chains, the DB-I to DB-IV contain 3 to 6 chains, respectively. All DBs share the same along-chain periodicity corresponding to a_0, but each exhibits a distinct atomic configuration. Within each DB, the chains display variations in apparent height, width, and interchain spacing in STM topography images.

DB-I and DB-III, which contain odd numbers of chains (3 and 5, respectively), exhibit mirror-symmetric atomic configurations and topographic contrast. Conversely, DB-II and DB-IV, which contain even numbers of chains (4 and 6), display asymmetric configurations, where one side consistently appears brighter in STM images. Taking DB-I as an example (Figure S1), the relative contrast of the chains may reverse under different biases or microtips, while sharp tips allow clear identification of atomic arrangements. Considering the edge chains as one part of the β_{12}-0° borophene lattice, DB-I shows a thinner chain in the center (Figure S1d,f), whereas DB-II contains two such chains, with one consistently brighter than the other one. Atomically resolved images suggest that DB-III can be understood as two DB-I structural units sharing one common borophene chain, as marked by the red arrow in Figure 2c. This assignment is consistent with its characteristic STM width of about 1.6 nm, which is approximately twice that of DB-I. Likewise, DB-IV can be understood as a combined DB-I and DB-II structural unit, with a width of about 2.0 nm, close to the sum of DB-I and DB-II. Statistical analysis indicates that DB-III is rarely observed and usually short, implying its metastable nature.

Beyond their structural diversity, all DBs exhibit a unified and unexpected superstructure modulation along the chain direction. This modulation has a period of 1.20 ± 0.06 nm, which is precisely four times the a_0 lattice constant. This 4-fold modulation can be directly identified in STM topography and dI/dV maps under various scanning biases. Depending on the applied bias and STM microtip, the modulation appears either very pronounced or more subtly visible. Representative dI/dV maps at specific biases showing clear 4-fold modulations are presented in Figure 1f–i, while more detailed data sets are provided in Figures S1–S8. Typically, such superlattice modulations may originate from moiré pattern, quantum well states, charge density waves (CDWs), or other strong correlation effects. However, the moiré pattern can be excluded here because the along-chain periodicity of the β_{12}-0° phase is identical to a_0 (~0.3 nm), which is close to the lattice constant of the direction Ag [1$\bar{1}$0] (~0.29 nm). The expected moiré supercell would therefore have a much larger periodicity (~7.8 nm), inconsistent with the observed 1.2 nm modulation. Moreover, these 4-fold modulations are exclusively observed at the DBs but not on the normal borophene regions, despite their identical along-chain periodicity. Bias-dependent dI/dV mappings (Figures S2,S4,S6 and S8) reveal that the modulation period remains constant across a wide range of biases, ruling out quantum well states. The possibility of a 1D CDW can also be excluded: according to Peierls transition theory, a CDW should induce a distinct U-shaped gap near the Fermi level, as previously reported for the mirro-twin DBs in $MoSe_2$ and $MoTe_2$.[26,27] In direct contrast, our dI/dV spectra exhibit no such gap signature (Figure S9). Furthermore, the persistence of the 4-fold modulation across a wide temperature range (from 77 K down to 5 K) lends strong support to a structural origin, rather than an electronically driven correlated phase that would typically exhibit significant temperature dependence.

Structural Models of the Domain Boundaries

To evaluate the possibility of the DBs being mixed-chain phase of borophene,[16,22−24] three candidate structural models for DB-I were constructed (Figure S10), which designated as MP-I to MP-III, respectively. Comparison between DFT simulations and experimental STM results shows that all three proposed structures disagree with experimental observations in terms of overall topography and boundary width. Furthermore, all proposed intermixing models fail to exhibit the 4-fold modulation observed in experiments. The absence of this key feature, along with the noted dimensional and topographic

https://doi.org/10.1021/jacs.5c23239
J. Am. Chem. Soc. XXXX, XXX, XXX−XXX

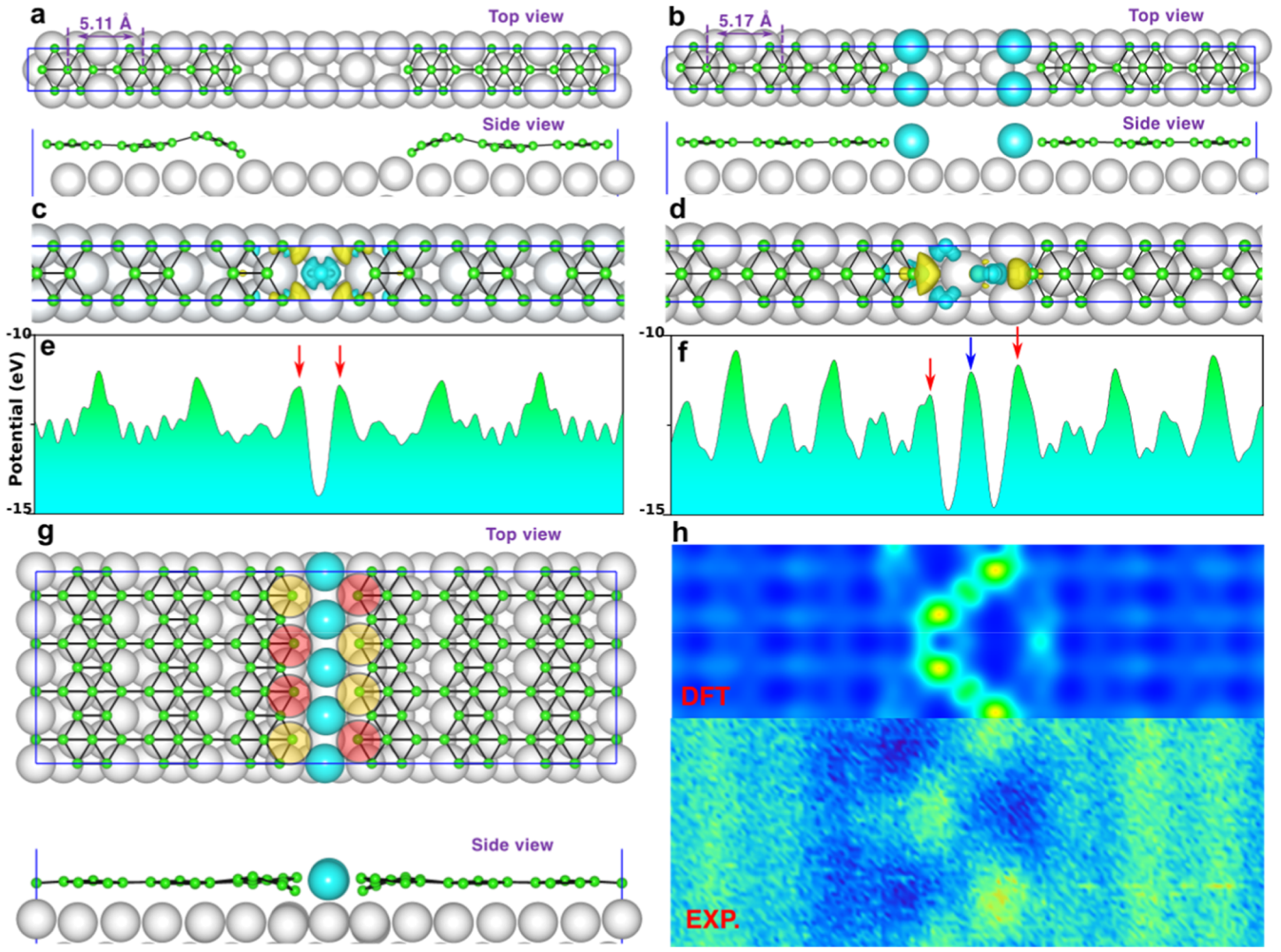

Figure 3. Structural and electronic characterization of borophene on Ag(111). (a) Structural model of open-edged borophene (six β_{12} chains) on an 8 × 1 orthogonal Ag(111) supercell. (b) Ag-decorated borophene under identical substrate conditions. (c,d) Isosurfaces (isovalue = 0.003 e/Å^3) of the charge density difference for DB-I and DB-II. (e,f) Electrostatic potential profiles perpendicular to the Ag chains across DB-I and DB-II. (g) Structural model of borophene (six chains) containing a boundary on a 7 × 4 Ag(111) supercell. Boundary Ag chains are shown in cyan; convex and concave borophene distortions are highlighted by red and yellow circles, respectively. (h) Simulated (top panel) and experimental (bottom panel) STS maps acquired at a sample bias of V_{tip} = −0.4 V and I = 200 pA. Yellow and cyan regions in (c,d) represent electron accumulation and depletion, respectively. To visualize charge transfer clearly in (c,d), the top-layer Ag atoms were scaled down to 1 Å in diameter and are thus concealed within the electron-depleted region (cyan isosurface).

inconsistencies, definitively excludes the mixed-chain phase scenario.

These findings guided us to consider a distinct possibility that the boundaries may not arise from borophene polymorphism alone, but instead involve the incorporation of substrate metal atoms. To implement this, a structural model for DB-I was constructed on a 12 × 1 Ag(111) substrate, featuring an 11 × 1 borophene overlayer with a single Ag atomic chain at the interface (Figures 2a and S11a). The B−Ag bond length measures 2.53 Å, while the β_{12}-0° chain distance is 5.22 Å, which matches experimental observations. The simulated STM image shows excellent agreement with the experimental data in both morphology and boundary width (Figure 2a). The analysis confirms that the bright central chain corresponds to an Ag atomic chain, while the edge chains belong to the β_{12}-0° borophene lattice. The calculated distance of 7.62 Å between the two edge chains matches the experimental boundary width d_1 = 0.80 ± 0.05 nm. Extending the concept of the Ag-chain boundary model from DB-I, structural models for DB-II to DB-IV were constructed as shown in Figures 2b−d and S11b−d. All models exhibit excellent agreement with experimental observations in both morphology and boundary width. Combined DFT and experimental STM analysis confirms that DB-II consists of two Ag atomic chains and β_{12}-0° borophene chains, with the brightest features corresponding to the Ag chains and the less bright ones to the β_{12}-0° lattice. Similarly, DB-III can be described as a combination of two DB-I units, featuring two Ag chains sandwiching a β_{12}-0° chain, where the brightest central chain is identified as the β_{12}-0° chain. DB-IV, in turn, represents a hybrid of DB-I and DB-II. To accommodate the inherent asymmetry of DB-IV while maintaining structural periodicity, additional Ag atoms were incorporated on both sides of the model (Figure S11d). All models exhibit excellent consistency with experimental observations in both morphology and boundary dimensions. Formation energies for all configurations were also calculated to assess the relative stability of the proposed models (Table S1). The DB structures are energetically favorable relative to the open-edge borophene (OE-B) configuration (see Figure 3a for its

https://doi.org/10.1021/jacs.5c23239
J. Am. Chem. Soc. XXXX, XXX, XXX−XXX

structural model), indicating that the incorporation of Ag atoms stabilizes the boundary under growth conditions. Among them, DB-I shows the lowest formation energy. In contrast, DB-III exhibits higher formation energy, suggesting its metastable nature, which agrees with the experimental observation that DB-III is relatively rare and short.

The analysis demonstrates that the interfacial intermixing of Ag atomic chains with borophene lattices consistently explains all experimentally observed boundary configurations. This mechanism, in which 1D metal chains coherently embed within a 2D host, parallels recent advances in confined single-metal-atom chains in transition metal dichalcogenides,[28] yet extends the concept to a metallic 2D system. Such atomically precise hybrid interfaces not only provide a platform for studying dimensionally confined quantum phenomena, but also establish a generalizable paradigm for fabricating mixed-dimensional heterostructures with tailored electronic properties.

Interfacial Bonding and Electronic Coupling

The structural contact between borophene and silver chains is identified as the key factor governing the geometric and electronic configuration of the interface. This is investigated using a model (open-edge borophene, OE-B) consisting of six periodic β_{12} borophene chains on a 7 × 1 Ag(111) substrate (Figure 3a). DFT calculations show that under-coordinated boron atoms at the borophene edge strongly interact with the Ag substrate, inducing pronounced edge wrinkling in the freestanding region with an interchain spacing of 5.11 Å. This effect remains consistent when the borophene layer is translated by half a substrate period along the *b*-axis (Figure S12a). Introducing Ag atoms at the borophene edge produces two distinct contact configurations (Figure 3b, S12b), which effectively suppress the initial wrinkling. This demonstrates the significant structural influence of Ag−B interactions. The associated Ag−B bond lengths are measured to be 2.30 Å and 2.21 Å, respectively. This reduction, compared to the 2.53 Å bond length in Figure 2a, is attributed to tensile strain within the system. Concurrently, the interchain distances increase to 5.17 Å and 5.12 Å, indicating the relief of structural stress from the initial wrinkling. The persistence of slight residual wrinkling and a marginally reduced chain spacing suggest locally confined strain due to the specific positions of the Ag atoms.

The introduction of Ag chains at borophene boundaries induces pronounced interfacial interactions. The charge transfer from the Ag atom at the domain boundary to the adjacent B atoms, quantified as 0.23 e^- by Bader analysis,[29] induces an interfacial dipole layer directed from B to Ag. This layer is associated with the formation of polar covalent bonds, as directly visualized in the charge density difference map (Figure 3c,d). This finding is further supported by theoretical studies of Ag−B clusters, which confirm strong covalent bonding via hybridization between Ag and B orbitals.[30,31] The resulting polar covalent bond could effectively bend the energy bands at the interface, thus lowering the contact barrier height. Electrostatic potential calculations reveal distinct interfacial landscapes for DB-I and DB-II. Specifically, symmetric contacts in DB-I produce a symmetric potential profile with the Ag−B contact potential (red arrow) lower than that of the B−B bond (Figure 3e). In contrast, the asymmetric DB-II exhibits two contact types, where type I shows a lower contact potential than the B−B bond, type II approaches the B−B bond potential, and the Ag−Ag bond potential (blue arrow) lies between them (Figure 3f). These electrostatic profiles directly govern the interfacial electronic behavior: the lower potential barrier at type I contacts facilitates efficient electron injection, suggesting suitability for Ohmic-like interfaces, while the higher barrier at type II may act as a charge-transport bottleneck. Furthermore, to elucidate the bonding mechanism at the interface, we analyzed the orbital-projected density of states (PDOS) for the Ag−B bond (Figure S13). A clear overlap between Ag and B states is observed near the Fermi level, indicating significant orbital hybridization. The B atom shows contributions from both *s* and *p* states, while the Ag states are dominated by *d* orbitals, with the d_{xy} component being the most prominent. This selective orbital overlap, particularly between Ag *d* states and B *s*/*p* states, reflects strong electronic coupling at the interface, highlighting the important role of Ag−B interactions in determining the local electronic structure. This distinction provides a key principle for designing borophene-metal interfaces with tailored electronic properties, enabling applications ranging from low-resistance contacts to gate-tunable junctions in future electronic devices.

To further quantify the interfacial charge redistribution, we also calculated the planar-averaged electrostatic potential along the surface normal for all systems. For DB-I, the electrostatic potential in the borophene region is noticeably higher than that of Ag(111) (Figure S14), indicating electron accumulation at the DB-I boundary. Correspondingly, the work function is calculated to be 4.45 eV for pristine Ag(111), while 4.92 eV for freestanding β_{12} borophene. This also indicates electrons will transfer from Ag(111) to borophene. The interfacial dipole moments are estimated to be ∼ 0.021, 0.004, 0.061, and 0.005 e·Å for DB-I to DB-IV, respectively, quantitatively confirming the formation of interfacial dipoles induced by DBs and supporting the charge transfer picture obtained from the Bader analysis.

The influence of Ag extends beyond borophene edges to induce notable structural modifications when Ag chains serve as internal boundaries. As borophene domains grow toward such a boundary from opposing sides, the confined space may be insufficient to accommodate a complete borophene unit, leading to the incorporation of Ag atoms within the constrained region. Nevertheless, this narrow boundary geometry can still introduce considerable local stress. To simulate this condition, a 6 × 4 borophene sheet was constructed on a 7 × 4 Ag(111) substrate, connected at the center by a 1 × 4 Ag chain, with an additional boron atom inserted at $x = 0$ to deliberately impose global compressive strain (Figure 3g). DFT calculations show that the resulting compression induces pronounced wrinkling in the borophene lattice near the boundary. This structural distortion leads to a quadrupling of the original periodicity along the Ag chain. Simulated STM images further reveal a zigzag electronic modulation exhibiting this 4-fold periodicity, in excellent agreement with experimental observations (Figure 3h). At monatomic step edges, STM/STS measurements (Figure S15) reveal a 2 × 1 superstructure at the borophene/Ag terrace interface, which is also reproduced by DFT calculations. This structure arises from the same compression-driven reconstruction mechanism as the 4 × 1 domain boundaries, while the different geometric constraints at the step edge lead to a shorter periodicity. This comprehensive investigation establishes that borophene-metal interactions create an atomically precise interface where geometric and electronic structures are

https://doi.org/10.1021/jacs.5c23239
J. Am. Chem. Soc. XXXX, XXX, XXX−XXX

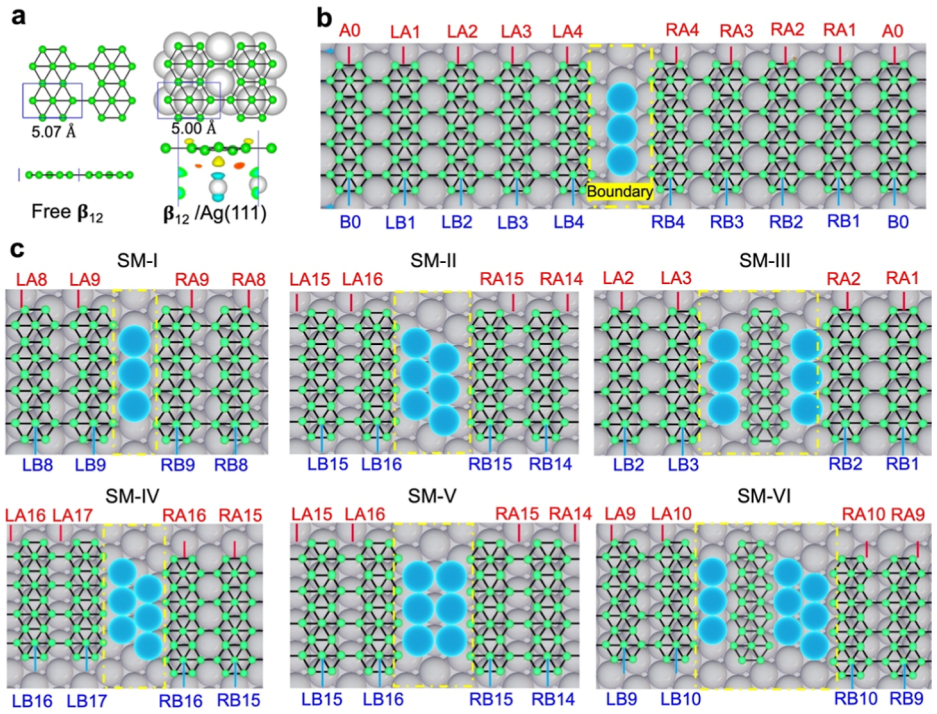

Figure 4. Formation mechanism of domain boundaries. (a) Atomic structure of freestanding β_{12} borophene (left) and borophene on a rectangular Ag(111) unit cell (right), with the corresponding charge density difference plots. Yellow and blue regions denote electron accumulation and depletion, respectively. (b) Schematic model illustrating the construction of borophene and Ag chain arrays on the Ag(111) surface. The notation LAn/RAn refers to Ag substrate units counted left/right from the origin, while LBm/RBm represents the corresponding borophene units. (c) Proposed atomic models for six types of boundaries (SM-I to SM-VI). Atoms are color-coded: cyan for Ag atoms within the boundary, green for B atoms, and gray for substrate Ag atoms.

mutually governed by interfacial bonding and stress regulation. The covalent Ag−B bonding not only stabilizes borophene edges but also enables the formation of well-defined 1D Ag chains that serve as internal boundaries. Most remarkably, these hybrid 1D-2D architectures exhibit tunable structural periodicity in the form of a quadrupled superstructure, along with the corresponding electronic modulations that perfectly match experimental observations. These findings provide fundamental insights into low-dimensional interface engineering and demonstrate the potential of borophene-templated structures as a versatile platform for designing quantum phases with tailored dimensionality and properties.

Formation Mechanism of the Ag-Embedded Boundaries

The formation mechanisms of the observed boundaries were elucidated by analyzing the structural evolution of β_{12}-0° borophene. Freestanding β_{12} borophene exhibits lattice constants of a = 2.93 Å and b = 5.07 Å (Figure 4a), consistent with previous theoretical studies.[32] Upon deposition on Ag(111), its lattice (b = 5.00 Å) shows initial registry but optimizes to a wrinkled structure, attributed to electron transfer from the substrate (0.04 e^- per B atom). The resulting interchain spacing (>5.1 Å) indicates inherent lattice mismatch with Ag(111). During growth, this mismatch prevents merging borophene domains from accommodating a complete unit at their boundaries. The geometric incompatibility is resolved by incorporating Ag atoms, whose arrangement dictates the boundary structure (Figure 4b). The Ag atoms constituting the embedded chains originate from the Ag(111) substrate itself under the elevated growth temperature (~400 °C). At such temperatures, the surface is highly dynamic, with a continuous population of mobile Ag adatoms available for incorporation into the growing borophene structure, a phenomenon commonly observed in surface-supported synthesis.[33−35] The dynamic Ag adatom population under growth conditions cannot be directly imaged by STM prior to deposition, as cooling the sample to imaging temperature fundamentally alters the equilibrium adatom concentration.

A lattice-mismatch-driven model was established to quantify boundary width W, defined as

$$W = (m' + n') \times 5.00 - (m + n) \times 5.17 + d_{B-B}$$

where d_{B-B} = 1.78 Å. Here, m and n are integers counting the number of borophene unit cells (LBm, RBn) on the left and right sides of the boundary, respectively. The corresponding integers m' and n' denote the number of Ag(111) substrate unit cells (LAm', RAn') over the same spatial interval. The value of 5.17 Å corresponds to the interchain spacing in the edge region of the structure shown in Figure 3b after relaxation, which is slightly larger than the intrinsic lattice constant due to edge effects and substrate interaction. For example, a single Ag-chain boundary (SM-I) requires a width of 3.66 Å, satisfied by $m + n$ = 18 and $m' + n'$ = 19 (Figure 4c). This structural requirement explains the tensile strain observed in the Figure 2a system, where an 11 × 1 borophene sheet is supported on a 12 × 1 Ag(111) substrate, resulting from the inherent lattice mismatch. Wider boundaries accommodate more complex structures, such as diatomic Ag chains (SM-II & V) or mixed Ag−B chains (SM-III). Asymmetric (SM-IV) and hybrid configurations (SM-VI) are also identified for wider or misaligned interfaces. This theoretical framework establishes a comprehensive mechanism for boundary formation, demonstrating how lattice mismatch and geometric constraints

https://doi.org/10.1021/jacs.5c23239
J. Am. Chem. Soc. XXXX, XXX, XXX−XXX

deterministically generate the diverse boundary configurations observed experimentally. The model successfully explains the structural variety and provides predictive capability for engineering the structure-property relationships of 2D material interfaces, as exemplified in metal-phosphorus networks.[36]

CONCLUSIONS

This work systematically investigates the synthesis and interaction mechanisms between borophene and metal at the atomic scale. Through combined STM measurements and DFT calculations, it is revealed that the distinct DBs observed in borophene β_{12} phase on Ag(111) are not intrinsic boron features but rather 1D Ag chains embedded within the 2D lattice. Four primary types of DBs are identified, each exhibiting a characteristic 4-fold periodic superlattice modulation along the borophene chains. At the DBs, Ag chains form an Ohmic contact with borophene. At these interfacial regions, charge transfer between Ag and B atoms leads to the formation of polar covalent Ag−B bonds, which exhibit a lower electrostatic potential than that of B−B bonds, thereby collectively facilitating efficient electron injection. Furthermore, the formation mechanism of these DBs is explained by a lattice-mismatch-driven model. Collectively, this study establishes the borophene/Ag(111) system as a model platform for understanding covalently bonded low-dimensional interfaces and demonstrates a substrate-mediated pathway for the bottom-up synthesis of atomically precise mixed-dimensional heterostructures.

METHODS

Experimental Methods

The experiments were performed in a home-built low-temperature STM system equipped with an MBE preparation chamber, with a base pressure better than 5×10^{-10} Torr. The Ag(111) substrates were cleaned by two cycles of Ar^+ sputtering at 1.0 kV followed by annealing at 600 °C for approximately 20 min. The boron was evaporated from a pure boron source using an electron beam evaporator operated at 70 W (1 kV, 70 mA), with a deposition rate of approximately 13.5 min per monolayer. Based on several samples grown at different deposition rates, we did not observe any obvious qualitative differences in either the borophene structures or the domain boundary structures. In contrast, the substrate temperature had a stronger effect on sample growth. The pure β_{12}-0° borophene phase studied here was obtained when the substrate was held at about 400 °C or slightly higher. At lower substrate temperatures, such as around 350 °C, mixed borophene phases of β_{12}-90° and χ_3 were formed without the Ag-chain-embedded domain boundaries, consistent with previous reports.[13] After growth, the sample was transferred to the STM stage without exposure to air. All STM/S measurements were conducted at 5 K. The dI/dV maps were recorded using the internal lock-in module of the Nanonis controller (f_{lockin} = 737 Hz, $V_{modulation}$ = 20 mV). All STM/S images were processed using the WSxM software.[37]

Computational Methods

First-principles calculations based on density functional theory (DFT) were performed to investigate the structural and electronic properties of the studied systems. All calculations were carried out using the Vienna Ab initio Simulation Package (VASP)[38,39] with the projector-augmented wave (PAW) method[40] and the Perdew-Burke-Ernzerhof (PBE)[41] generalized gradient approximation exchange-correlation functional. A plane-wave basis set with an energy cutoff of 500 eV was employed. The Brillouin zone was sampled with a Monkhorst-Pack k-point mesh[42] ensuring a k-spacing of no greater than $2\pi \times 0.02$ Å^{-1} in all directions for structural optimization. The energy convergence criterion was set to 10^{-5} eV, and atomic positions were relaxed using the conjugate gradient algorithm until the maximum force on each atom was less than 0.01 eV Å^{-1}. The Ag(111) surface was modeled by a three-layer slab with a vacuum gap of at least 18 Å. During structural optimization, the bottom layer was fixed at the bulk positions, while the top two Ag layers and all adsorbate atoms were fully relaxed. As a representative example, the DB-I structure was constructed using a three-layer Ag(111) slab containing 78 Ag atoms. The borophene overlayer consists of 60 B atoms (corresponding to 12 β_{12} units) and one interfacial Ag atom forming the Ag chain. The lateral supercell dimensions are 65.05 Å × 2.89 Å. Similar slab thickness and modeling strategies were adopted for all other DB configurations. Electronic structure analysis was performed following structural relaxation. Dipole corrections along the surface normal direction were applied in all slab calculations to eliminate spurious electrostatic interactions between periodic images. STM images were simulated using the Tersoff-Hamann approximation based on partial charge densities obtained from VASP calculations.[43,44] For each simulation, the bias voltage was set to match the corresponding experimental value by integrating the local density of states from the Fermi level to the energy corresponding to the sample bias.

ASSOCIATED CONTENT

Supporting Information

The Supporting Information is available free of charge at https://pubs.acs.org/doi/10.1021/jacs.5c23239.

STM characterization of type-I domain boundaries (DB-I); Bias-dependent dI/dV maps of the type-I domain boundary (DB-I); STM images of type-II domain boundaries (DB-II); Bias-dependent dI/dV maps of the type-II domain boundary (DB-II); STM images of type-III domain boundaries (DB-III); Bias-dependent dI/dV maps of the type-III domain boundary (DB-III); STM images of type-IV domain boundaries (DB-IV); Bias-dependent dI/dV maps of the type-IV domain boundary (DB-IV); dI/dV spectra and DFT calculated DOS; Three proposed structural models for intermixing configurations; Structural models of DBs used for STM simulation; Formation energies; Structural models of borophene on Ag(111); PDOS for interfacial Ag and B atoms in the DB-I structure; Planar-averaged electrostatic potential of DB-I; Borophene at the upper Ag terrace (PDF)

AUTHOR INFORMATION

Corresponding Authors

Zhenpeng Hu − *School of Physics, Nankai University, Tianjin 300071, People's Republic of China;* orcid.org/0000-0002-8469-1683; Email: zphu@nankai.edu.cn

Lan Chen − *Institute of Physics, Chinese Academy of Sciences, Beijing 100190, People's Republic of China; School of Physical Sciences, University of Chinese Academy of Sciences, Beijing 100190, People's Republic of China;* orcid.org/0000-0003-4426-9944; Email: lchen@iphy.ac.cn

Authors

Qian Gao − *College of Information Science and Engineering, Shandong Agricultural University, Tai'an 271000, People's Republic of China*

Wenbin Li − *Institute of Physics, Chinese Academy of Sciences, Beijing 100190, People's Republic of China; School of Physical Sciences, University of Chinese Academy of Sciences, Beijing 100190, People's Republic of China;* Present Address: Department of Chemistry, National University

https://doi.org/10.1021/jacs.5c23239
J. Am. Chem. Soc. XXXX, XXX, XXX−XXX

of Singapore, Singapore 117543, Singapore; orcid.org/0000-0002-3147-3893

Caiyun Chen − *Institute of Physics, Chinese Academy of Sciences, Beijing 100190, People's Republic of China; School of Physical Sciences, University of Chinese Academy of Sciences, Beijing 100190, People's Republic of China*

Kehui Wu − *Tsientang Institute for Advanced Study, Zhejiang 310024, China;* orcid.org/0000-0002-7698-5673

Complete contact information is available at: https://pubs.acs.org/10.1021/jacs.5c23239

Author Contributions

#Q.G. and W.L. contributed equally to this work.

Notes

The authors declare no competing financial interest.

■ ACKNOWLEDGMENTS

This work was financially supported by the Ministry of Science and Technology (MOST) of China (Grant No. 2024YFA1409100), the National Natural Science Foundation of China (Grant Nos.T2325028, 12134019, 21773124), the Shandong Provincial Natural Science Foundation (ZR2024QA178, ZR2022MA087), and L.C. acknowledges the support from the CAS Project for Young Scientists in Basic Research (Grant No. YSBR-054).

■ REFERENCES

(1) Li, W.; et al. Approaching the quantum limit in two-dimensional semiconductor contacts. *Nature* **2023**, *613*, 274.
(2) Luo, L.; Gao, J.; Zheng, L.; Li, L.; Li, W.; Xu, M.; Jiang, H.; Li, Y.; Wu, H.; Ji, H.; et al. Ultra-low power consumption flexible sensing electronics by dendritic bilayer MoS2. *InfoMat* **2024**, *6*, No. e12605.
(3) Liu, C.; et al. A full-featured 2D flash chip enabled by system integration. *Nature* **2025**, *646*, 1081.
(4) Gao, L.; et al. Atomic layer bonding contacts in two-dimensional semiconductors. *Science* **2025**, *390*, 813.
(5) Liu, X.; et al. Contact resistance and interfacial engineering: Advances in high-performance 2D-TMD based devices. *Prog. Mater. Sci.* **2025**, *148*, 101390.
(6) Zhang, Z.; Yang, Y.; Penev, E. S.; Yakobson, B. I. Elasticity, Flexibility, and Ideal Strength of Borophenes. *Adv. Funct. Mater.* **2017**, *27*, 1605059.
(7) Macilon, P. G. C. A.; Santos, T. F.; Santos, E. V.; Carvalho, B. R.; Nascimento, J. H. O. Advances in 21st century on borophene-based nanomaterials for next-generation energy technologies. *Emergent Mater.* **2025**, *8*(6), 3893−3934.
(8) Wu, X.; Dai, J.; Zhao, Y.; Zhuo, Z.; Yang, J.; Zeng, X. C. Two-Dimensional Boron Monolayer Sheets. *ACS Nano* **2012**, *6*, 7443.
(9) Liu, Y.; Penev, E. S.; Yakobson, B. I. Probing the Synthesis of Two-Dimensional Boron by First-Principles Computations. *Angew. Chem., Int. Ed.* **2013**, *52*, 3156.
(10) Qiu, L.; Zhang, X.; Kong, X.; Mitchell, I.; Yan, T.; Kim, S. Y.; Yakobson, B. I.; Ding, F. Theory of sigma bond resonance in flat boron materials. *Nat. Commun.* **2023**, *14*, 1804.
(11) Ou, M.; Wang, X.; Yu, L.; Liu, C.; Tao, W.; Ji, X.; Mei, L. The Emergence and Evolution of Borophene. *Adv. Sci.* **2021**, *8*, 2001801.
(12) Li, W.-L.; Jian, T.; Chen, X.; Chen, T.-T.; Lopez, G. V.; Li, J.; Wang, L.-S. The Planar CoB18− Cluster as a Motif for Metallo-Borophenes. *Angew. Chem., Int. Ed.* **2016**, *55*, 7358.
(13) Feng, B.; et al. Experimental realization of two-dimensional boron sheets. *Nat. Chem.* **2016**, *8*, 563.
(14) Mannix, A. J.; et al. Synthesis of borophenes: Anisotropic, two-dimensional boron polymorphs. *Science* **2015**, *350*, 1513.
(15) Zhong, Q.; et al. Synthesis of borophene nanoribbons on Ag(110) surface. *Phys. Rev. Mater.* **2017**, *1*, 021001.
(16) Wang, Y.; Kong, L.; Chen, C.; Cheng, P.; Feng, B.; Wu, K.; Chen, L. Realization of Regular-Mixed Quasi-1D Borophene Chains with Long-Range Order. *Adv. Mater.* **2020**, *32*, 2005128.
(17) Wu, R.; Eltinge, S.; Drozdov, I. K.; Gozar, A.; Zahl, P.; Sadowski, J. T.; Ismail-Beigi, S.; Božović, I. Micrometre-scale single-crystalline borophene on a square-lattice Cu(100) surface. *Nat. Chem.* **2022**, *14*, 377.
(18) Wu, R.; Drozdov, I. K.; Eltinge, S.; Zahl, P.; Ismail-Beigi, S.; Božović, I.; Gozar, A. Large-area single-crystal sheets of borophene on Cu(111) surfaces. *Nat. Nanotechnol.* **2019**, *14*, 44.
(19) Li, W.; et al. Experimental realization of honeycomb borophene. *Sci. Bull.* **2018**, *63*, 282.
(20) Kiraly, B.; Liu, X.; Wang, L.; Zhang, Z.; Mannix, A. J.; Fisher, B. L.; Yakobson, B. I.; Hersam, M. C.; Guisinger, N. P. Borophene Synthesis on Au(111). *ACS Nano* **2019**, *13*, 3816.
(21) Vinogradov, N. A.; Lyalin, A.; Taketsugu, T.; Vinogradov, A. S.; Preobrajenski, A. Single-Phase Borophene on Ir(111): Formation, Structure, and Decoupling from the Support. *ACS Nano* **2019**, *13*, 14511.
(22) Liu, X.; Zhang, Z.; Wang, L.; Yakobson, B. I.; Hersam, M. C. Intermixing and periodic self-assembly of borophene line defects. *Nat. Mater.* **2018**, *17*, 783.
(23) Liu, X.; Wang, L.; Li, S.; Rahn, M. S.; Yakobson, B. I.; Hersam, M. C. Geometric imaging of borophene polymorphs with functionalized probes. *Nat. Commun.* **2019**, *10*, 1642.
(24) Liu, L.; Zhang, Z.; Liu, X.; Xuan, X.; Yakobson, B. I.; Hersam, M. C.; Guo, W. Borophene Concentric Superlattices via Self-Assembly of Twin Boundaries. *Nano Lett.* **2020**, *20*, 1315.
(25) Zhang, Z.; Mannix, A. J.; Hu, Z.; Kiraly, B.; Guisinger, N. P.; Hersam, M. C.; Yakobson, B. I. Substrate-Induced Nanoscale Undulations of Borophene on Silver. *Nano Lett.* **2016**, *16*, 6622.
(26) Barja, S.; et al. Charge density wave order in 1D mirror twin boundaries of single-layer MoSe2. *Nat. Phys.* **2016**, *12*, 751.
(27) Wang, L.; et al. Direct Observation of One-Dimensional Peierls-type Charge Density Wave in Twin Boundaries of Monolayer MoTe2. *ACS Nano* **2020**, *14*, 8299.
(28) Qin, W.; Guo, S.; Liu, Z.; Zhang, P.; Zhu, C.; Wu, Y.; Qiao, R.; Liu, Z.; Guo, W.; Zhang, Z. Coherently confined single-metal-atom chains in 2D semiconductors. *Nat. Commun.* **2025**, *16*, 4924.
(29) Sanville, E.; Kenny, S. D.; Smith, R.; Henkelman, G. Improved grid-based algorithm for Bader charge allocation. *J. Comput. Chem.* **2007**, *28*, 899.
(30) Dong, X.; Chen, C.; Cui, Z.-h. Tuning structural preference of negatively charged B16 by ionically or covalently interacting with alkali and coinage metals. *Chem. Phys.* **2021**, *550*, 111315.
(31) Fu, P.; Chen, B.; Sun, W.; Lu, C. Theoretical investigations on structural evolution, photoelectron spectroscopy and electronic properties of precious metal silver doped boron clusters. *Phys. Lett. A* **2025**, *548*, 130553.
(32) Gao, M.; Li, Q.-Z.; Yan, X.-W.; Wang, J. Prediction of phonon-mediated superconductivity in borophene. *Phys. Rev. B* **2017**, *95*, 024505.
(33) Patel, S. B.; Li, C.; Al-Mahboob, A.; Sadowski, J. T.; Zhou, G. Effects of Temperature Fluctuations on Surface Mobility of Atomic Steps and Oxidation Dynamics in High-Temperature Alloys. *J. Am. Chem. Soc.* **2025**, *147*, 1656.
(34) Li, L.; Schultz, J. F.; Mahapatra, S.; Liu, D.; Zhang, X.; Jiang, N. Optical Spectroscopic Probing and Atomic Visualization of the Motion of N-Heterocyclic Carbenes on Ag(111). *ACS Nano* **2025**, *19*, 15363.
(35) Zhong, Q.; Niu, K.; Chen, L.; Zhang, H.; Ebeling, D.; Björk, J.; Müllen, K.; Schirmeisen, A.; Chi, L. Substrate-Modulated Synthesis of Metal-Organic Hybrids by Tunable Multiple Aryl−Metal Bonds. *J. Am. Chem. Soc.* **2022**, *144*, 8214.
(36) Tian, H.; et al. Two-Dimensional Metal-Phosphorus Network. *Matter* **2020**, *2*, 111.
(37) Horcas, I.; Fernández, R.; Gómez-Rodríguez, J. M.; Colchero, J.; Gómez-Herrero, J.; Baro, A. M. WSXM: A software for scanning

probe microscopy and a tool for nanotechnology. *Rev. Sci. Instrum.* **2007**, *78*, 013705.
(38) Kresse, G.; Furthmüller, J. Efficiency of ab-initio total energy calculations for metals and semiconductors using a plane-wave basis set. *Comput. Mater. Sci.* **1996**, *6*, 15.
(39) Kresse, G.; Furthmüller, J. Efficient iterative schemes for ab initio total-energy calculations using a plane-wave basis set. *Phys. Rev. B:Condens. Matter* **1996**, *54*, 11169.
(40) Blöchl, P. E. Projector augmented-wave method. *Phys. Rev. B:Condens. Matter* **1994**, *50*, 17953.
(41) Perdew, J. P.; Burke, K.; Ernzerhof, M. Generalized Gradient Approximation Made Simple. *Phys. Rev. Lett.* **1996**, *77*, 3865.
(42) Monkhorst, H. J.; Pack, J. D. Special points for Brillouin-zone integrations. *Phys. Rev. B:* **1976**, *13*, 5188.
(43) Tersoff, J.; Hamann, D. R. Theory and Application for the Scanning Tunneling Microscope. *Phys. Rev. Lett.* **1983**, *50*, 1998.
(44) Tersoff, J.; Hamann, D. R. Theory of the scanning tunneling microscope. *Phys. Rev. B:Condens. Matter* **1985**, *31*, 805.

https://doi.org/10.1021/jacs.5c23239
J. Am. Chem. Soc. XXXX, XXX, XXX−XXX